A Plant Tendril-Like Soft Robot That Grasps and Anchors by Exploiting its Material Arrangement

Fabian Meder, *Member, IEEE*, Saravana Prashanth Murali Babu, and Barbara Mazzolai, *Member, IEEE*

***Abstract*—Some climbing plants use tendrils as efficient strategies to anchor and support their weights while they move in unstructured environments. In this letter, we mimic the essential functions of tendrils that wrap around the support in a soft state by a spiral winding (coiling) and then lignify or stiffen to strengthen the attachment. We implement a simple hierarchical pre-programmed functionality at the material level using off-the-shelf materials and easy fabrication methods to achieve coiling and stiffening and incorporate an electrical control. The resulting robots hence consist of a bilayer of silicone elastomers that encapsulate a thermoplastic core and a heating element. The bilayer that spontaneously forms a helically coiled configuration in its equilibrium state is controlled by a solid-to-liquid phase transition of the thermoplastic core upon resistive heating. Integrating these mechanisms into a single structure allows mimicking the basic tendril functions. Our realization is a straightforward assembly with electrical control that offers the perspective to be a building block for soft robots that require controllable attachment solutions such as growing artifacts and devices that operate in unstructured environments, e.g., operating in vegetation.**

***Index Terms*—Biologically-inspired robots, soft robot materials and design, biomimetics.**

I. Introduction

CLIMBING plants use efficient attachment strategies to attach their bodies to a support as they grow thus reducing the amount of organic material needed to reach great heights [1]–[4]. Tendrils, elongated structures that wrap around a support in response to trigger are a common mechanism for plant attachment in unstructured environments (Fig. 1). The tendrils coil helically around a scaffold by asymmetric contraction of fibers in their structure, which results in attachment to that scaffold [3]. The coiling is initiated by specialized cells that sense contact with the scaffold [5]. In this case, the asymmetric contraction is probably the result of differential lignification, variations in the orientation of cellulose fibrils, or differential water affinities leading to unequal water output by some cells, which causes increased cell contraction [3]. After coiling, the tendril material lignifies, which leads to a considerable stiffening of the tissue and thus to a further strengthening of the attachment.

Fig. 1. Photographs of the coiled tendrils of *Lagenaria siceraria*, also known as bottle gourd, which the climbing plant uses to anchor and attach to different supports.

Soft robots are gaining rapid momentum, since they are safe when interacting with living beings, or able to handle delicate objects, abilities that have been gaining more popularity in robotics research. Progress in plant and especially tendril-inspired soft robotics has enhanced the derivation of functionalities adapted from the plant behavior that will have significant effect on environmental applications, such as remote exploration, monitoring agriculture, fixture for vegetation or crop handling, biomedical applications, and many more [4], [6]–[10].

Several robots and actuators have already been developed that mimic the tendril-like coiling behavior [7]–[9], [11]–[15] by using combination of an interaction between materials and structural arrangement. This approach in soft robots is usually realized in two ways: (i) using flexible and complaint systems including pneumatics [16], [17], hydraulics [18], and tendon-driven systems [19]; (ii) using smart materials and stimuli responsive actuation like magnetic [20], light [21], [22], heat [23], [24], humidity [25], [26] and osmosis [12]. Of these, flexible and compliant devices are robust but they are limited to actuation source such as pumps and motors. Well-controlled stiffness variation can for example be achieved by temperature-controlled phase transitions [27]. Advanced materials have the

Manuscript received October 11, 2021; accepted February 8, 2022. Date of publication February 23, 2022; date of current version March 11, 2022. This letter was recommended for publication by Associate Editor E. W. Hawkes and Editor K.-J. Cho upon evaluation of the reviewers' comments. This work was supported by the European Union's Horizon 2020 Research and Innovation Programme through Project GrowBot under Grant Agreement 824074. *(Fabian Meder and Saravana Prashanth Murali Babu contributed equally to this work.) (Corresponding authors: Fabian Meder; Saravana Prashanth Murali Babu; Barbara Mazzolai.)*

Fabian Meder and Barbara Mazzolai are with the Bioinspired Soft Robotics, Istituto Italiano di Tecnologia, 16163 Genoa, Italy (e-mail: fabian.meder@iit.it, barbara.mazzolai@iit.it).

Saravana Prashanth Murali Babu was with the Bioinspired Soft Robotics, Istituto Italiano di Tecnologia, 16163 Genoa, Italy. He is now with SDU Biorobotics, University of Southern Denmark, 5230 Odense, Denmark (e-mail: spmb@mmmi.sdu.dk).

This letter has supplementary downloadable material available at https://doi.org/10.1109/LRA.2022.3153713, provided by the authors.

Digital Object Identifier 10.1109/LRA.2022.3153713

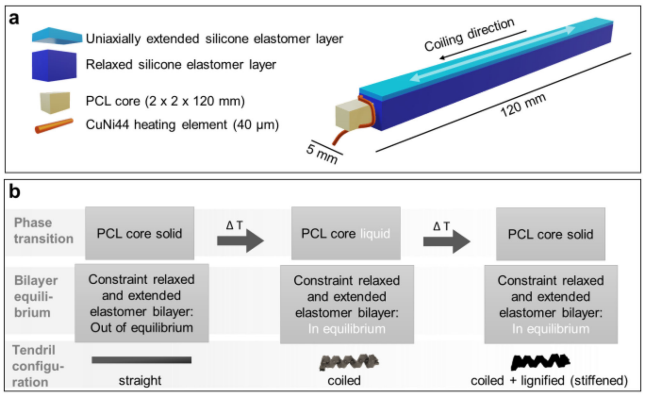

Fig. 2. Design and components and working principle of the artificial tendril. (a) Overview of the key components obtained by 3D printing (PCL core), and silicone elastomer casting (silicone elastomer bilayer). (b) Block diagram describing the phase transition and resulting changes in the bilayer equilibrium and tendril configuration.

functionality to actuate and, when specifically designed to do so, to reversibly attach/interlock with freestanding supports [28]. However, many solutions often require specific materials and production capabilities, and sometimes thin layers which may not support high grasping forces. In particular, the integration with electrically controlled triggering of the attachment would facilitate the integration of such attachment solutions in more complex robots. Electroactive polymers and shape memory alloys have promising features suitable to articulating soft robots [7], [29]. Yet, limitations include the output force, high operating voltages, and to some extent a challenging production.

The aim of this work was thus to extract the essential functions of tendrils and mimic them in a straightforward device based on the integration of one component of a basic "physical intelligence" [30] at the material level through "pre-programming" the materials and controlling their equilibrium states, as described in the following sections.

The proposed system (Fig. 2(a)) uses polycaprolactone (PCL) as variable stiffness element due to its phase transition at a low melting point (∼60 °C). Moreover, it is non-toxic, biodegradable, and 3D-printable. Silicone elastomers were chosen to store/release elastic energy due to their excellent elasticity and tear strength as well as the ease-of-application by common techniques. The system is fabricated by standard soft robot production techniques, like molding and casting strategies and 3D printing to facilitate fabrication and make the devices compatible with other soft robots.

At the same time, we integrate the capability to trigger the coiling electrically enabling the control with standard electronics and providing a way to eliminate complex external systems, such as pumps in pneumatic actuation, motors in tendon driven systems, etc. The results are easily fabricated devices that provide tendril-like coiling, permanent attachment, and reinforcement through a lignification-like behavior achieving high gripping forces and electrical control. In the future, these devices can be equipped with sensors to detect supports and integrated into complex robots that require permanent attachment strategies to free-standing supports.

II. Design and Working Principle of the Artificial Tendril – A Simple Hierarchical Pre-Programmed Functionality

The proposed tendril-like soft robot is based on a "programmed" material, which has its equilibrium state in the coiled helical configuration. This can be achieved by tightly bonding elastomer layers in different extended/stretched states, resulted in a configuration that resembles asymmetrically contracted tendril fibers. Two silicone elastomer layers (here we chose the EcoFlex 0030, SmoothOn), one uniaxially stretched and one remaining in the relaxed state, were bonded together and constrained to form a helical structure driven by the interaction between the stretched and the relaxed layers. The result is a bilayer material that spontaneously forms a helically coiled configuration in its equilibrium state.

Now, to control the coiling, the bilayer material is brought out of equilibrium by adding a stiffer core that overcomes the coiling forces thus preventing coiling and resulting in a physically straight material. We chose a 3D-printed rectangular rod of thermoplastic PCL (2 mm × 2 mm × 120 mm) as the core material, which is also used as a phase transition element. PCL has the advantage of being a biodegradable polyester with a low melting point of about 60°C. Therefore, its phase transition from the solid to the liquid state can be triggered at relatively low temperatures. In the solid state, the PCL rod is dimensioned to withstand the forces exerted by the elastomeric bilayer. However, when transitioning to the liquid state, the PCL core no longer balances the forces exerted by the elastomer constraint, allowing for coiling. To achieve the phase transition, we incorporated a resistive heating element in form of a 40 μm CuNi44 wire around the PCL core, which can be heated by applying a current to the heating element until the phase transition occurs. The phase transition then leads to instantaneous coiling. After coiling and when heating is interrupted, the PCL core cools and eventually returns to the solid state (Fig. 2(b)). This leads to a stiffening of the coiled structure, which mimics the lignification process occurring in the plant's tendril (variation of cell walls to strengthen the plant tissue) and improves attachment forces being much faster than the natural counterpart.

III. Fabrication and Experiments

A. Fabrication

The PCL cores were 3D printed in dimensions of 2 × 2 × 120 mm with an infill density of 30% using a Prusa MK3 printer (Prusa Research a.s, Czech Republic) and a PCL filament (Facilan^{TM} PCL 100 Filament, 3D4Makers, The Netherlands). In order to integrate a heating element, a 40 μm CuNi44 wire (Evek GmbH, Germany) with a length of typically 60 cm, was wound around the PCL cores in a self-made winding device consisting of a motor coupled to a ball bearing on one end and a free moving ball bearing on the other end. The PCL core was fixed between them like a shaft to achieve a homogeneous rotation around its central axis. In this way, homogeneous windings of the CuNi44 wire were obtained at different winding densities. A thin layer of superglue was applied to the PCL core to promote the adhesion of the heating element to the core.

Casting of the silicone bilayer was performed as follows. First, a thin layer (∼0.5 mm) of silicone rubber prepolymer (Ecoflex 0030, SmoothOn, USA) was mixed in a 1:1 ratio according to the supplier's instructions to obtain a final volume of ∼120 ml, casted onto polymethyl methacrylate sheet (PMMA) (60 × 40 cm) and cured for 24 hours. Pieces of approximately 10 × 30 cm of the cured elastomer layer were then cut and stretched to the desired extension and fixed in the stretched state on a PMMA sheet (10 × 15 cm) by attaching them to the edges of sheet with adhesive tape. Subsequently, the second, relaxed elastomer layer was merged with the stretched layer using the following approaches. For the analysis of the bilayer, no PCL core was used and a second layer was merged by applying a thin layer of Ecoflex 0030 prepolymer to the stretched elastomer as an adhesive for merging the second relaxed layer of the previously casted unstretched silicone elastomer to the stretched layer and cured for 24 hours and then cut into pieces of typically ∼5 × 120 mm. Two equivalent methods were used to integrate the PCL cores and the heating element: (i) the PCL core was placed on the extended silicone rubber layer attached to the PMMA substrate, and Ecoflex 0030 was poured on top to fix an unstretched layer on top of the stretched layer with a sandwiched PCL core (wrapped with the heating element). After a curing time of 24 hours, the excess elastomer was cut off with a blade cutter to obtain the integrated tendril-like device. (ii) a second method to fabricate the integrated tendrils was to use a 3D-printed rectangular prism mold (4 mm × 4 mm × 120 mm) in which the PCL core with the heating element was fixed. A silicone elastomer layer was then cast around the PCL core resulting in a 1 mm thick elastomer coating of the PCL core taking after curing and serving as the relaxed elastomer layer. Subsequently, the PCL core coated in this way was bonded with Ecoflex 0030 to an extended silicone elastomer layer (fabricated and fixed as described above) and cured for 24 hours. Excess silicone elastomer was cut.

B. Experiments

The heating element was powered in all experiments by a standard digital power supply (RS-3000, RSPro, United Kingdom) at the indicated voltages. The temperature variations of the PCL core during heating and phase transition were thermographically recorded using a FLIR A325sc thermal imaging camera (FLIR System AB, Sweden) and analyzed using FLIR Research IR Max software (version 3.5.13277.1001). Three point bending tests were performed on the PCL cores using a dedicated 3D printed setup consisting of support pillars and an indenter. The PCL core was placed on top of the pillars at equal lengths and the indenter was directly screwed to a 6-DOF load cell (Nano17, ATI). Indentation was performed by using digitally controlled linear stage (M-111 Compact Micro-Translation Stage, PI). Before each measurement, the readings of the load cell were offset to provide a common reference. For all the experiments, measurements were repeated at least five times. The data was analyzed and plotted in MATLAB, Version 2019b (MathWorks Inc., USA).

IV. Results and Discussion

A. Properties of the Coiling Elastomer Bilayer

Fig. 3(a) and Fig. 3(b) show the equilibrium state of the silicone elastomer bilayers (shore hardness 0030) obtained by varying different parameters during their fabrication steps. Fig. 3(a) shows bilayers obtained by varying the degree of extension of the pre-stretched layer compared to the relaxed layer. It is expected that higher pre-stretch ratio increases the coiling force due to larger elastic deformation acting on the bilayer. Fig. 3(b), respectively shows bilayers obtained by varying the angle keeping pre-stretch percentage constant in which the two layers were joined. This has expectedly an influence both on the helix formation and angle, which depend thus on the angle that the two elastomer layers formed when they were merged. Accordingly, structures merged at 0° would theoretically "roll up" or have a helix angle of 0°. Yet, as the structure's width is relative short compared to its length, during rolling, the layers slide off resulting in a helical coil. Especially at larger variations of the merging angle, the effect becomes significant. For example, coiling is completely lost when the bilayers are not uniaxially merged (0°) but instead merged at 90° which is typically used to obtain bistable matrices but not coiling. Fig. 3(c) shows the influence of the length of the bilayer (diameter 5 mm) on the number of helical turns in the equilibrium coil. The number of turns increases with the total length. Fig. 3(c) shows that, for the given dimensions (5 mm × 120 mm), the pre-stretch has no influence on the number of turns, and Fig. 3(d) confirms that the angle at which the two layers were merged affect the number of turns in the coil only at angles far from the uniaxial case, i.e., at 90°. The results indicate that coiling occurs in all tested cases in the equilibrium state of the uniaxial elastomer bilayers and that the dimensions have a key influence on the number of turns in the structures.

B. Properties of the Phase Transition Structure

Fig. 4(a) shows the PCL core (2 mm × 2 mm × 120 mm) with the integrated CuNi44 heating element. Different winding densities with different winding angles were realized to test which configuration leads to the fastest and most homogeneous heating of the PCL to reach the temperature of its phase transition from the solid to the liquid state (∼60 °C). This leads to the required stiffness variation that enables the tendril-like coiling of the final devices. Fig. 4(b) shows thermal images representing the heat distributions in the different structures with diverse winding densities of the heating elements after applying a voltage of 30 V for 15 s. As expected, higher winding densities lead to more homogeneous heating of the PCL core structure and it avoids regions that are far from the phase transition temperature. We then measured the stiffness variation upon heating by measuring the indentation force required to move a cantilever pushing the sample downwards to a displacement of 5 mm in a three-point bending configuration after applying a certain voltage to the heating element for 20 s. The results are shown in Fig. 4(c). At the given heating duration, lower voltages, 5 V and 10 V, do not show any significant variation of the indentation force related to

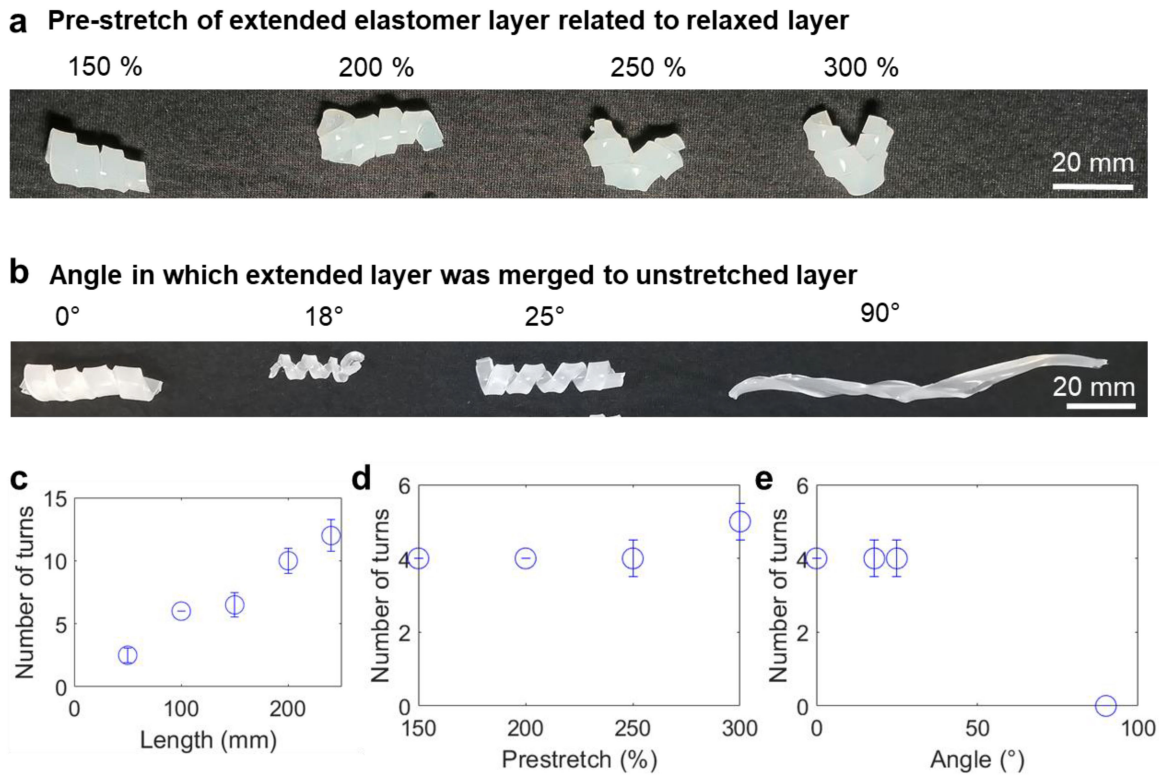

Fig. 3. Coiling characteristics of the elastomeric bilayer in equilibrium state as function of different design parameters. (a) Images of the equilibrium state of the coiling elastomeric bilayer as function of pre-stretch applied to the extended layer in relation to the relaxed layer. (b) Images of the equilibrium state of the coiling elastomeric bilayer as function of the angle in which the uniaxially extended and the relaxed layer were merged. (c) Number of turns of the coil as function of length of the bilayer in equilibrium state (diameter 5 mm, pre-stretch 200%). (d) Number of turns of the coil as function of prestretch of the extended layer in relation to the relaxed layer (diameter 5 mm, length 120 mm). (e) Number of turns of the coil as function of angle in which the two layer have been merged (diameter 5 mm, length 120 mm, pre-stretch 200%). The datapoints represent the average of five measurements per conditions, error bars represent the standard deviations.

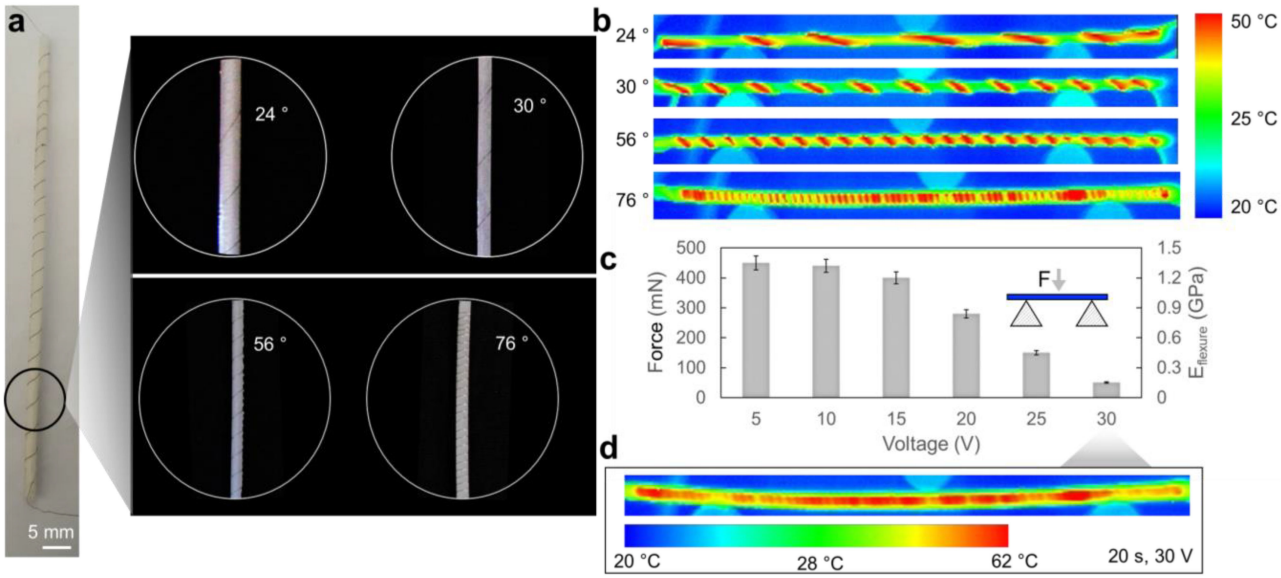

Fig. 4. Properties of the PCL core with integrated heating elements. (a) Photographs of the the PCL core (2 mm × 2 mm × 120 mm) combined with the CuNi44 resistive heating wire applied in different densities and winding angles onto the cores. (b) Thermal imaging showing different heat distribution in the PCL cores with different windings after a voltage of 30 V (0.27 A) was applied to the heating element for 15 s. (c) Stiffness variation of the PCL core due to the phase transition displayed as variation of the indentation force and the corresponding flexural modulus, $E_{flexure}$, in a three-point bending test as function of the voltage applied to the heating element with the highest winding density (76° winding angle) for 20 s. Then the current was switched off and the force measured. (d) Thermal image of the PCL core at the moment the current was turned off showing homogenous heating to ∼60 °C (PCL melting point) after applying 30 V for 20 s.

PCL phase transition. However, further increasing the voltage to > 10 V leads to faster heating of the heating element and a change in stiffness. The heat Q produced by resistive heating is given by the Joule's first law

$$Q = \frac{V^2}{R}t \tag{1}$$

where V is the applied voltage, R the resistance of the heating element and t the time. This relationship is evident in the decrease of the indentation force at higher voltages, which clearly indicates the phase transition of the PCL core towards a less viscous, liquid state. Indeed, applying 30 V for only 20 s results in the lowest forces associated with the lowest stiffness. Fig. 3(d) shows the homogeneous heat distribution in the PCL core after heating for 20 s at 30 V at highest winding density (76° winding angle) taken immediately after switching off the power supply. The image shows that the core has reached a temperature of ∼60 °C which corresponds to the melting point of PCL and the measured forces clearly indicate stiffness change and phase transition of PCL. Under these conditions, the PCL core in a device in which the core is integrated with the elastic bilayer is expected to permit the elastic deformation of the bilayer and hence trigger coiling in contrast to its solid state hindering elastic deformation. This behavior was then tested in the integrated artificial tendrils.

C. Functions of the Integrated, Electrically Triggerable Soft Artificial Tendrils

After characterizing the coiled equilibrium state of the elastomer bilayer and the phase transition of the PCL cores, we combined both structures and mechanisms to obtain an integrated actuation whose behavior is mainly determined by the physical properties of its constituent materials. Fig. 5(a) illustrates the simple structure, the electrical circuit, and hence the key components of the fully functional, integrated, soft artificial tendril. Fig. 5(b) shows the coiling of the tendril around a support indicating the different states of the materials that lead to this behavior. In the linear state, before electrically triggering the heating, the PCL is in the solid phase preventing coiling of the elastic bilayer which is hence out of equilibrium. When the current is switched on, heating of the PCL core leads to the phase transition and stiffness variation. Now, the coiling starts as the liquid PCL core permits the bilayer deformation aiming for its equilibrium state and the tendril coils around a suitable support. Switching off the current leads to cooling of the PCL core below its melting point inducing the liquid-solid phase transition. The solidification of the PCL takes place in about 30 s after turning the current off whereas the PCL remains still in the coiled conformation determined by the elastic memory during the liquid state. The stiffening of the PCL resembles the lignification process in the natural tendril and strengthens the attachment. Movie 1 shows the performance of artificial tendrils wrapped around supports in real-time. Fig. 5(c) compares the y-component of the tendril motion from the video with the timing of the electrical triggering and the resistive heating. The tendril moves in the heating phase and does not further change the position, when the power supply is turned off. The heat produced due to resistive heating was calculated using Joules first law with equation (1) for different input voltages showing that expectedly during a heating period of 30 s, more heat can be produced by higher voltages. Heat dissipation in the PCL and in the environment plays thereby further roles. Yet, the voltage is thereby a critical factor which controls tendril behavior and can be used to tune it. For example, if faster coiling is preferred, higher voltages are required, if slower coiling is sufficient, lower voltages can be used (here by applying 30 V, coiling around the support finished in ∼30 s). Yet, the power consumption at such conditions ∼8 W applied for only 30 s can be considered as total energy consumption of 67 mWh (2.2 mAh) required to implement permanent attachment by such a tendril structure. Indeed, before coiling and once coiling occurred, no energy input is necessary as the material combination uses the energy stored in the elastic bilayer and the PCL core. This may have an energetic benefit obtained by the pre-programmed functionality compared to devices which would need to power also the actuation instead of only the phase transition but our system may be also further improved by reducing consumption. Moreover, the artificial tendril after lignification provides a grasping force sufficient to hold over 160 times its own weight and at least 3.1 N with one winding around a support and 5.4 N with two windings, respectively (Fig. 5(e)). The maximum grasping force will be studied in detail in future investigations but the estimations already show that implementing the stiffening or "lignification" of the core is crucial to achieve high grasping forces as both, one or two windings, respectively could not hold the given weights before lignification.

As in the natural tendril, the attachment of our artificial tendril is in the final state irreversible and once attached, it remains fixed on the structure. This makes the devices "one-shot" systems fully dedicated to achieving a permanent and long-term attachment to a support, similarly to the natural counterpart. Still, a feature to release the artificial version could be easily implemented in the future by applying another heating cycle to melt the core and applying a sufficient force to unwrap the tendril in the soft state from the support. It depends on the desired application, if attachment (and release) or reversible grasping is desired. For the latter, other solutions like fluidic-driven systems would have benefits. The speed of the devices could be improved by optimizing the size of the tendril and core dimensions in respect of the final grasping force needed. This could reduce the material that needs to heat up to achieve the phase transition, thus enabling faster response (the system in the current state is already orders of magnitude faster than the natural tendril that requires days to coil and lignify). One of the key features that we aim to integrate in a next generation of the artificial tendrils is a sensitive skin that can determine between different supports in terms of dimensions, materials, and trigger. Natural tendrils not only can sense touch, but some climbing plants can also distinguish between physical structures, materials, and for example volatile chemicals in the environment that somewhat direct the decision in an unstructured environment towards which support is suitable and which not [5], [31]. Such complex sensing functionality is highly desired in artificial systems but difficult to realize

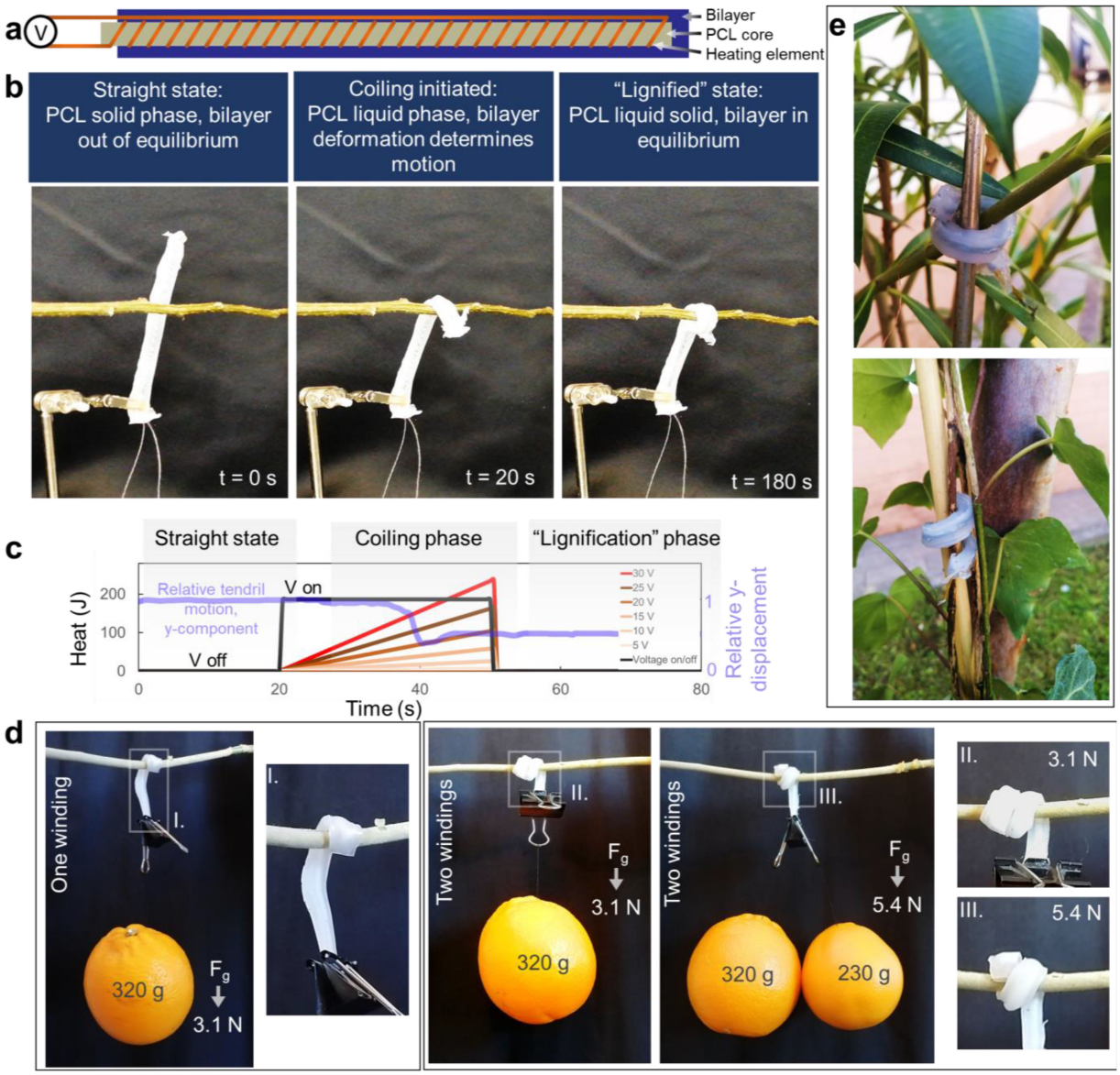

Fig. 5. Integrated soft artificial tendrils and electrically triggered coiling. (a) Schematic of the simple structure of the artificial tendril leading to controlled coiling behavior using mainly physical properties of the integrated materials. (b) Snapshots of Movie 1 showing the tendril behavior during different states as indicated above the images. (c) Comparison of the y-component of the tendril motion (from Movie 1) with the timing of the electrical trigger and the heat produced by resistive heating as function of time. The three states, straight state, coiling phase, lignification phase programmed by the physical properties of the tendril materials are highlighted. The resistive heating only triggers the PCL phase transition, and actuation is enabled by the materials configuration. (d) Example of the grasping force of artificial tendrils after "lignification" with one winding (left panel) and two windings (right panel) around a support (diameter 5 mm). One winding can sustain a weight of 320 g (3.1 N), which corresponds to 160 times the tendrils own weight (2 g). With two windings it can even sustain 550 g (5.4 N). (e) Photographs of plants (*N. oleander* upper image and *H. helix*, lower image, respectively) which do not have own tendrils were fixed with the artificial tendrils to pillars supporting the plant growth.

especially if complex touch or chemical sensors, which require further power supplies or tethering other devices, cannot be used to maintain minimal complexity. Moreover, to compensate the fact that single tendrils may not always be successful in finding and coiling around a suitable support, climbing plants typically produce multiple tendrils on a single branch that aim for the goal to fix the plant to a supporting structure. Thereby reducing complexity and integrating functionality at the material level is crucial. Developing materials with integrated sensing functionalities [28], [30] will help to overcome such issues and represent a great benefit to realize autonomous artificial tendrils that are capable to differentiate suitable supports in unstructured or unknown environments.

Fig. 5(d) shows one of several application scenarios in which plants (*N. oleander* upper image and *H. helix*, lower image, respectively), which do not have own tendrils were fixed to pillars supporting the plant growth. Here, the artificial tendril assumes the task of a natural tendril. This can be interesting in supporting the agriculture sector. However, we believe that another interesting application scenario is in the field of robotics

and self-growing artifacts, especially robots that build their own body or build non-predetermined structures in unstructured environments [7], [10], [32]–[35]. Again, the function of the artificial tendril would be the same as in plants and help the robot or growing artifact during motion to reduce energy by anchoring to and using supports available in direct proximity.

V. Conclusion

By programming the equilibrium states and phase transitions of materials in elastic bilayers and low-melting point polymers and couple their functionalities in a single structure, we could create a pre-programmed functionality that mimics the properties of plant tendrils, actuates, and varies stiffness. The characteristic coiling around a support could be triggered in our artificial tendrils by an electrical control to enable or block the autonomous actuation and coiling of the artificial tendril. All processes have been realized using standard soft robotic fabrication techniques and 3D-printing, without the need to synthesize complex materials. The final artificial tendrils are a proof of concept and a starting point for developing a plant-inspired long-term attachment strategy that can in future be sensorized, e.g., by touch sensors, and integrated in robots that need to operate in unstructured environments.

Appendix

Movie 1 shows the real time coiling of artificial tendrils around a support.

Acknowledgment

All authors acknowledge the support from the project GrowBot, the European Union's Horizon 2020 Research and Innovation Programme under Grant Agreement No. 824074.

References

[1] N. P. Rowe and T. Speck, "Stem biomechanics, strength of attachment, and developmental plasticity of vines and lianas," *Ecology of Lianas*, vol. 2014, pp. 323–341, 2014.

[2] J. N. Burris, S. C. Lenaghan, and C. N. Stewart, "Climbing plants: Attachment adaptations and bioinspired innovations," *Plant Cell Rep.*, vol. 37, no. 4, pp. 565–574, 2018.

[3] S. J. Gerbode, J. R. Puzey, A. G. McCormick, and L. Mahadevan, "How the cucumber tendril coils and overwinds," *Sciance (80-.)*, vol. 337, no. 6098, pp. 1087–1091, 2012.

[4] I. Fiorello, E. Del Dottore, F. Tramacere, and B. Mazzolai, "Taking inspiration from climbing plants: Methodologies and benchmarks - A review," *Bioinspiration Biomimetics*, vol. 15, no. 3, 2020, Art. no. 031001.

[5] J. Braam and J. Braam, "In touch - plant responses to mechanical stimuli," *New Phytol.*, vol. 165, no. 2, pp. 373–389, 2005.

[6] B. Mazzolai, L. Beccai, and V. Mattoli, "Plants as model in biomimetics and biorobotics: New perspectives," *Front. Bioeng. Biotechnol.*, vol. 2, no. 2, pp. 1–5, Jan. 2014.

[7] J. Gallentine, M. B. Wooten, M. Thielen, I. D. Walker, T. Speck, and K. Niklas, "Searching and intertwining: Climbing plants and Growbots," *Front. Robot. AI*, vol. 7, no. 118, pp. 1–14, Aug. 2020.

[8] M. B. Wooten and I. D. Walker, "Vine-inspired continuum tendril robots and circumnutations," *Robotics*, vol. 7, no. 3, 2018, Art. no. 58.

[9] D. Nahar, P. M. Yanik, and I. D. Walker, "Robot tendrils: Long, thin continuum robots for inspection in space operations," in *Proc. IEEE Aerosp. Conf.*, 2017, pp. 1–8.

[10] B. Mazzolai, A. Mondini, E. Del Dottore, and A. Sadeghi, "Self-growing adaptable soft robots," in *Mechanically Responsive Materials For Soft Robotics*, Hoboken, NJ, USA: Wiley, 2019, pp. 363–394.

[11] W. Wang, C. Li, M. Cho, and S. H. Ahn, "Soft tendril-inspired grippers: Shape morphing of programmable polymer-paper bilayer composites," *ACS Appl. Mater. Interfaces*, vol. 10, no. 12, pp. 10419–10427, 2018.

[12] I. Must, E. Sinibaldi, and B. Mazzolai, "A variable-stiffness tendril-like soft robot based on reversible osmotic actuation," *Nature Commun.*, vol. 10, no. 1, pp. 1–8, 2019.

[13] M. Wang, B. P. Lin, and H. Yang, "A plant tendril mimic soft actuator with phototunable bending and chiral twisting motion modes," *Nature Commun.*, vol. 7, pp. 1–8, 2016.

[14] S. Sareh *et al.*, "Bio-inspired tactile sensor sleeve for surgical soft manipulators," in *Proc. IEEE Int. Conf. Robot. Automat.*, 2014, pp. 1454–1459.

[15] K. Sonaike, S. M. Hadi Sadati, C. Bergeles, and I. D. Walker, "Exploiting the morphology of a shape memory spring as the active backbone of a highly dexterous tendril robot (ATBR)," in *Proc. IEEE/RSJ Int. Conf. Intell. Robots Syst.*, 2020, pp. 8801–8806.

[16] S. P. M. Babu, A. Sadeghi, A. Mondini, and B. Mazzolai, "Antagonistic pneumatic actuators with variable stiffness for soft robotic applications," in *Proc. IEEE Int. Conf. Soft Robot.*, 2019, pp. 283–288.

[17] J. Walker *et al.*, "Soft robotics: A review of recent developments of pneumatic soft actuators," *Actuators*, vol. 9, 2020, Art. no. 3.

[18] R. K. Katzschmann, A. D. Marchese, and D. Rus, "Hydraulic autonomous soft robotic fish for 3D swimming," *Springer Tracts Adv. Robot.*, vol. 109, pp. 405–420, 2016.

[19] J. Choi, S. H. Ahn, and K. J. Cho, "Design of fully soft actuator with double-helix tendon routing path for twisting motion," in *Proc. IEEE Int. Conf. Intell. Robot. Syst.*, 2020, pp. 8661–8666.

[20] E. B. Joyee and Y. Pan, "A fully three-dimensional printed inchworm-inspired soft robot with magnetic actuation," *Soft Robot.*, vol. 6, no. 3, pp. 333–345, 2019.

[21] F. Meder, G. A. Naselli, A. Sadeghi, and B. Mazzolai, "Remotely light-powered soft fluidic actuators based on plasmonic-driven phase transitions in elastic constraint," *Adv. Mater.*, vol. 31, no. 51, pp. 1–8, 2019.

[22] S. Iamsaard *et al.*, "Conversion of light into macroscopic helical motion," *Nature Chem.*, vol. 6, no. 3, pp. 229–235, 2014.

[23] F. Visentin, S. P. Murali Babu, F. Meder, and B. Mazzolai, "Selective stiffening in soft actuators by triggered phase transition of hydrogel-filled elastomers," *Adv. Funct. Mater.*, vol. 31, no. 32, 2021, Art. no. 2101121.

[24] V. Sanchez *et al.*, "Smart thermally actuating textiles," *Adv. Mater. Technol.*, vol. 5, no. 8, pp. 1–10, 2020.

[25] A. K. Bastola, N. Rodriguez, M. Behl, P. Soffiatti, N. P. Rowe, and A. Lendlein, "Cactus-inspired design principles for soft robotics based on 3D printed hydrogel-elastomer systems," *Mater. Des.*, vol. 202, 2021, Art. no. 109515.

[26] B. Shin *et al.*, "Hygrobot: A self-locomotive ratcheted actuator powered by environmental humidity," *Sci. Robot.*, vol. 3, no. 14, pp. 1–9, 2018.

[27] L. Sullivan, I. D. Walker, K. Althoefer, and T. Nanayakkara, "Three-Dimensional-Printable thermoactive helical interface with decentralized morphological stiffness control for continuum manipulators," *IEEE Robot. Automat. Lett.*, vol. 3, no. 3, pp. 2283–2290, Jul. 2018.

[28] J. Xiong, J. Chen, and P. S. Lee, "Functional fibers and fabrics for soft robotics, wearables, and human–robot interface," *Adv. Mater.*, vol. 33, no. 19, pp. 1–43, 2021.

[29] M. Hao, Y. Wang, Z. Zhu, Q. He, D. Zhu, and M. Luo, "A compact review of IPMC as soft actuator and sensor: Current trends, challenges, and potential solutions from our recent work," *Front. Robot. AI*, vol. 6, no. 129, pp. 1–7, Dec. 2019.

[30] M. Sitti, "Physical intelligence as a new paradigm," *Extreme Mechanics Lett.*, vol. 46, 2021, Art. no. 101340.

[31] Y. Fukano, "Vine tendrils use contact chemoreception to avoid conspecific leaves," *Proc. Roy. Soc. B: Biol. Sci.*, vol. 284, 2017, Art. no. 1850.

[32] A. Sadeghi, A. Mondini, and B. Mazzolai, "Toward self-growing soft robots inspired by plant roots and based on additive manufacturing technologies," *Soft Robot.*, vol. 4, no. 3, pp. 211–223, 2017.

[33] E. Del Dottore, A. Sadeghi, A. Mondini, V. Mattoli, and B. Mazzolai, "Toward growing robots: A historical evolution from cellular to plant-inspired robotics," *Front. Robot. AI*, vol. 5, no. 16, Mar. 2018, Art. no. 16.

[34] E. W. Hawkes, L. H. Blumenschein, J. D. Greer, and A. M. Okamura, "A soft robot that navigates its environment through growth," *Sci. Robot.*, vol. 2, no. 8, pp. 1–8, 2017.

[35] A. Sadeghi, E. Del Dottore, A. Mondini, and B. Mazzolai, "Passive morphological adaptation for obstacle avoidance in a self-growing robot produced by additive manufacturing," *Soft Robot.*, vol. 7, no. 1, pp. 85–94, 2020.